Heliyon 7 (2021) e06646

Contents lists available at ScienceDirect

Heliyon

journal homepage: www.cell.com/heliyon

Research article

Exploring the molecular structure, vibrational spectroscopic, quantum chemical calculation and molecular docking studies of curcumin: A potential PI3K/AKT uptake inhibitor

M. Govindammal [a], M. Prasath [a,*], S. Kamaraj [b], S. Muthu [c], M. Selvapandiyan [a]

[a] Department of Physics, Periyar University PG Extension Centre, Dharmapuri, 636701, India
[b] Department of Biotechnology, Periyar University PG Extension Centre, Dharmapuri, India
[c] Department of Physics, Arignar Anna Govt. Arts College, Cheyyar, 604407, Tamilnadu, India

ARTICLE INFO

Keywords:
FT-IR
FT-Raman
ADMET prediction
Molecular dynamics and molecular Docking

ABSTRACT

The IUPAC name of curcumin is (1E, 6E)-1,7-Bis(4-hydroxy-3methoxyphenyl) hepta-1,6-e-3,5-dione (7B3M5D) and is characterized by spectroscopic profiling with FT-IR and FT-Raman spectra obtained both experimentally and theoretically. PED analysis was done for the confirmation of minimum energy obtained in the title compound. Optimized geometrical parameters are compared with experimental values obtained for 7B3M5D by utilizing B3LYP functional employing 6–311++G (d,p) level of theory. The HOMO-LUMO, MEP, and Fukui function analysis has been used to elucidate the information regarding charge transfer within the molecule. The stabilization energy and charge delocalization of the 7B3M5D were performed by NBO analysis. This article assesses that the title compound act as a potential inhibitor of the PI3K/AKT inhibitor through in silico studies, like molecular docking, molecular dynamics (MD), ADMET prediction and also this molecule obeys Lipinski's rule of five. 7B3M5D was docked effectively in the active site of PI3K/AKT inhibitor.

1. Introduction

Abnormality in the cells, which is the body's basic unit of life, results in Cancer. One of the most deadly cancers in the world is Lung Cancer [1]. Lung cancer is otherwise called Lung carcinoma. Like any other cancer type, Lung cancer also arises due to the uncontrolled growth of cells in Lung tissues. Tobacco smoking, gene expression, atmospheric pollution, past disease history and occupational exposure are the leading causes of Lung cancer worldwide.

The Phosphoinositide 3-Kinase (PI3K/AKT/mTOR) is a major part of the signaling cascade, which is commonly deactivated in cancers [2, 3]. Hence, Disparities in the PI3K/AKT pathway make an order of important contribution and growth of lung cancer, the regulation of the PI3K/AKT pathway can stimulate the transduction of many downstream signals. Also, PI3K is activated to be involved in several cell signaling cascades to regulate diverse of cancer cell proliferation, cell growth, apoptosis, cell differentiation [4, 5]. AKT, alongside Phosphoinositide 3-Kinase, are the pivotal parts of the Tyrosine Kinase signaling cascade and it acts as PI3K/AKT signaling, this signaling way stimulates cell survival and growth factors. The results also give proof that the 7B3M5D inhibits the growth of non-small cell lung cancer (NSCLC) is to develop anti-cancer drugs [6]. The PI3K family is one group of kinases that has become a current attraction of drug discovery [7, 8].

The Biologically active compound curcumin is an extract from *Curcuma longa* plants with yellow-colored phenolic antioxidant [9] with molecular formula $C_{21}H_{20}O_6$. According to in vivo studies, it has been previously demonstrated that 7B3M5D is a potent inhibitor of the PI3K signaling pathway [10]. The present work aims to provide a detailed explanation of the 7B3M5D molecule by both theoretically and experimentally observed values. The computational and observed IR and Raman intensities spectrum is compared with the estimated vibrational assignments. Further HOMO-LUMO, Molecular Electrostatic Potential, Density of State (DOS) were analyzed. The local reactivity descriptors such as Mulliken atomic charge, local softness, and Fukui function and electrophilicity index were determined. The ADMET prediction and drug-likeness profile gives the information about pharmacokinetic and toxicity properties of the 7B3M5D molecule, which are determined to discover its drug potential. The molecular dynamics (MD) simulation has been performed for 20 ns timescale on free PI3K/AKT inhibitor and protein-ligand complex to assess their properties of structural dynamics

* Corresponding author.
E-mail address: sanprasath2006@gmail.com (M. Prasath).

https://doi.org/10.1016/j.heliyon.2021.e06646
Received 29 January 2021; Received in revised form 16 March 2021; Accepted 26 March 2021

and stability of the molecule. Molecular docking examination is utilized to predict protein-ligand complexes, intermolecular and hydrogen bonding interactions of the 7B3M5D molecule with the PI3K inhibitor with PDB ID: (4FA6). The title compound is effectively used as anti-Non Small Cell Lung Cancer.

2. Materials and methods

2.1. Experimental details

The title compound with purity above 98% was procured from Sigma Aldrich Company. The Fourier transform infrared spectrum of 7B3M5D was recorded in the region 4000-400 cm^{-1} using the KBr pellet technique with resolution of 1.0 cm^{-1}. Further, the FT-Raman spectrum has been recorded in the region 4000-100 cm^{-1} with 2 cm^{-1} resolution using Brucker RFS 27 at Nd: YAG (Neodymium-doped aluminum garnet) laser source of 1064 nm at SAIF-IIT, Chennai.

2.2. Computational details

The molecular structure of 7B3M5D was optimized through the DFT method with a 6–311++G (d,p) basis set by using the Gaussian 09W program [11]. Theoretical vibrational assignments for 7B3M5D are described by PED % which is done by the VEDA program package [12]. In this current work a scaling factor value of 0.961 was utilized for the B3LYP/6–311++ (d, p) level of theory [13]. Second-order Fock Matrix regulates the donor-acceptor interactions for 7B3M5D and is computed through NBO 3.1 program [14]. The energy distribution from HOMO-LUMO is determined using the Gaussview [15]. 7B3M5D exhibits nucleophilic and electrophilic nature which was elucidated by Molecular Electrostatic Potential (MEP), Mulliken atomic charges, and Fukui Function reactivity. Autodock (1.5.6 version) was used to study the molecular docking evaluation [16]. Cygwin software is used to produce the protein-ligand complex. The PyMOL [17] and Discovery Studio software was used to view the protein-ligand complex.

3. Results and discussion

3.1. Molecular geometry

The molecular structure of 7B3M5D belongs to C_1 point group symmetry and displays the optimized molecular structure of 7B3M5D with the numbering scheme of the atom as shown in (Figure 1). The molecular structural parameters are computed by using B3LYP functional with 6–311++G (d, p) level of theory. The computed parameters of bond length and bond angle for the 7B3M5D molecule are compared with experimental values [18] which are presented in (Table 1). The theoretical values for the title compound were closely related to the experimental results. Also, the computed optimized values of the 7B3M5D molecule exhibit that the bond lengths of O(8)-C(3) and O(9)-C(5) are found to be 1.212 and 1.212Å (theoretical) and has been slightly varied from the experimental values 1.214 and 1.216 Å (experimental). The higher bond lengths of the ketone group present in the title molecule are found to be C(3)-C(4) and C(4)-C(5) at a distance of 1.525, 1.531 Å (theoretical), and 1.412, 1.384 Å (experimental). This deviation in the title molecule bond length and bond angle suggests the bonding nature of the atom.

3.2. Vibrational assignments

The 7B3M5D comprises 47 atoms, with 135 emblematic modes of vibrations. The vibrational assignments of 7B3M5D have been concluded with PED analysis. The spectral analysis of the observed FT-IR and FT-Raman spectra and theoretical spectra of both are shown (Figure 2 (a&b)). The computed scaled frequency, IR intensity, Raman activity, and vibrational assignments of the title compound are presented in Table 2.

3.2.1. C–C vibrations

The ring C–C symmetric stretching vibrations are attributed in the range between 1600 to 1400 cm^{-1} [19,20] for the aromatic and hetroaromatic compound. The bands which are of various intensities were ascertained in FT-IR spectrum at 1589, 1504 cm^{-1}, and FT-Raman bands were identified at 1609, 1510 and 949 cm^{-1}, respectively. The computed values were achieved in the range of 1622, 1589, 1587, 1572, 1566, 1513, 1128, and 939 cm^{-1} by the B3LYP/6–311++G (d, p) method with a maximum PED contribution of 54%.

3.2.2. C–H vibrations

The C–H symmetric stretching vibrations are exhibited in the spectral range between 3100–3000 cm^{-1}, which is the distinctive region for the identification of the aromatic C–H symmetric stretching vibrations [21, 22]. The absorptions of bands are not affected substantially by the nature of constituents. The aromatic C–H symmetric stretching bands of the 7B3M5D molecule is theoretically specified in the range 3103, 3097, 3094, 3082, 3069, 3068, 3055,3053,3050, 3036, 3034,3021,3018, 2972,2957, 2924 and 2906 cm^{-1}, which shows good agreements with the bands observed in the reported FT- IR spectrum at 2978 and 2904

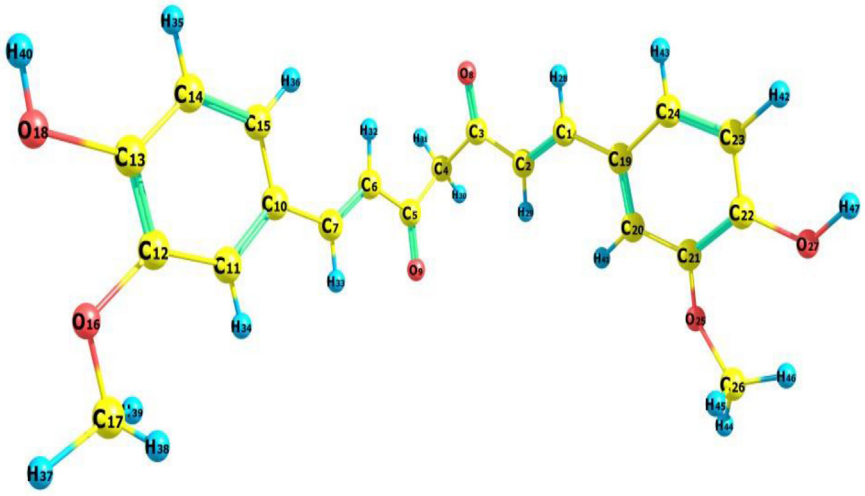

Figure 1. Optimized geometrical structure with atomic labeling of 7B3M5D.

Table 1. Selected geometrical parameters (Bond length (Å), Bond angle (°) and Torsion angle (°)) of Curcumin.

Parameters	Calculated	Experimental
Bond length (Å)		
O(8)-C(3)	1.212	1.214
O(9)-C(5)	1.212	1.216
C(2)-C(1)	1.351	1.330
C(2)-C(3)	1.467	1.467
C(3)-C(4)	1.525	1.412
C(4)-C(5)	1.531	1.384
C(5)-C(6)	1.467	1.457
C(6)-C(7)	1.352	1.327
C(12)-O(16)	1.386	1.326
C(13)-O(18)	1.385	1.387
O(16)-C(17)	1.452	1.432
C(4)-H(30)	1.088	1.086
C(4)-H(31)	1.090	1.092
C(2)-H(29)	1.082	1.080
C(21)-O(25)	1.392	1.372
C(22)-O(27)	1.391	1.352
O(25)-C(26)	1.469	1.438
O(18)-H(40)	0.972	0.923
Bond Angle (°)		
O(8)-C(3)-C(4)	119.9	121.4
O(8)-C(3)-C(2)	123.0	120.1
C(4)-C(3)-C(2)	116.4	118.6
C(6)-C(5)-C(4)	116.6	121.6
O(9)-C(5)-C(4)	119.9	121.5
O(9)-C(5)-C(6)	123.3	118.0
C(5)-C(6)-C(7)	121.2	120.5
C(5)-C(4)-H(30)	107.5	106.4
C(3)-C(4)-H(31)	109.7	108.2

Experimental values taken from ref [18].

cm^{-1} and with the FT-Raman bands at 3037 and 2920 cm^{-1}. The maximum PED is 98% as shown in Table 2.

3.2.3. O–H vibrations

Generally the hydroxyl group of O–H symmetric stretching vibration has been found in the range between 3600-3400 cm^{-1} [23]. In present work, the O–H bands are observed in the IR spectrum at 3566 cm^{-1}. The O–H symmetric stretching vibrations are theoretically observed in peaks at 3579 and 3573 cm^{-1}, respectively. The maximum PED contribution is 100% implying it to be a pure symmetric stretching vibration. The computed values show clear agreement with the experimental data.

3.2.4. C–O vibrations

Generally, the C=O stretching vibration of COOH groups is correctly coincidens with the C=O stretch in ketones, which is assessed in the range 1740–1660 cm^{-1} [24]. The C–O symmetric stretching vibrations occur in the range from 1300-1000 cm^{-1} [25]. The peaks analogous to C–O symmetric stretching vibration are found at 1637, 1549, and 1234 cm^{-1} by B3LYP functional with employing 6–311++G (d,p) level of theory. Experimentally, it is observed in FT-IR spectrum at 1628 cm^{-1}, the Raman bands were recorded at 1520, 1232 cm^{-1}, the maximum PED is 67%.

3.2.5. Other vibrations

In FT-IR the symmetric bending vibrations of HCC are observed at 1406,1282, 1230 and 1210 cm^{-1} and FT-Raman spectra are observed at 1331 and 1242 cm^{-1}. The FT-IR torsional vibrations of HCCC are observed at 949, 854 and 807 cm^{-1} and FT-Raman bands have appeared at 843 cm^{-1}. Moreover, the OCC and CCC symmetric bending bands are observed at 573, 533 and 572 cm^{-1} for FT-IR and FT-Raman bands were recorded at 976, 467 and 220 cm^{-1}. OCCC out bands are recorded 630 cm^{-1} for FT-IR and 657, cm^{-1} for FT-Raman. All the vibrations of 7B3M5D were prepared and the detected values are in good agreement with the experimental values [26].

3.3. HOMO-LUMO

The excited-state energy of a molecule implicates the disparity between HOMO-LUMO which plays a crucial role in the chemical stability of the structure [27]. HOMO is Highest Occupied Molecular Orbital and LUMO is Lowest Unoccupied Molecular Orbital; corresponding to ionization potential and electron affinity. The HOMO-LUMO energies have been determined at B3LYP/6–311++G (d, p) level of the theory of (ΔE), EP→ Electron Affinity, IP→ Ionization Potential, χ→ Electronegativity, η→ Global Hardness, μ→ Chemical Potential and the S→ Softness (Eqs. (1), (2), (3), (4), and (5)) for 7B3M5D [28, 29], and the results are displayed in (Table 3) and (Figure 3), Where:-

$$\text{Chemical potential}(\mu) = \frac{1}{2}(E_{LUMO} + E_{HOMO}) \quad (1)$$

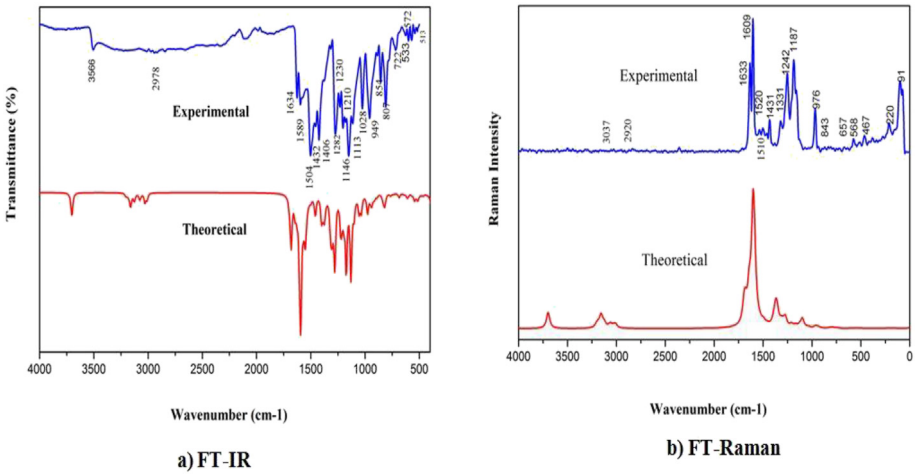

Figure 2. a) FT-IR and b) FT-Raman spectra of 7B3M5D (Experimental & Theoretical).

Table 2. Observed and calculated vibrational frequency of 7B3M5D at B3LYP method with 6–311++G (d,p) basis set.

Species	Observed Wavenumbers(cm-1)		Theoretical wave number (cm-1)		IR Intensity		Raman Intensity		
	FTIR	FT RAMAN	Unscaled Frequency	Scaled Frequency	Rel	Abs	Rel	Abs	Vibrational Assignments
W(135)			3702	3579	80	10	352	8	υ OH (100)
W(134)	3566		3695	3573	80	10	328	7	υ OH (100)
W(133)			3209	3103	2	0	30	1	υ CH (98)
W(132)			3202	3097	3	0	61	1	υ CH (92)
W(131)			3199	3094	10	1	31	1	υ CH (85)
W(130)			3187	3082	13	2	98	2	υ CH (88)
W(129)			3174	3069	11	1	14	0	υ CH (95)
W(128)			3173	3068	2	0	10	0	υ CH (85)
W(127)			3160	3055	14	2	92	2	υ CH (60)
W(126)			3157	3053	27	3	124	3	υ CH (88)
W(125)			3157	3053	23	3	124	3	υ CH (93)
W(124)			3154	3050	24	3	158	3	υ CH (92)
W(123)		3037	3139	3036	2	0	30	1	υ CH (98)
W(122)			3138	3034	3	0	26	1	υ CH (98)
W(121)			3124	3021	15	2	77	2	υ CH (63)
W(120)			3121	3018	38	5	82	2	υ CH (26)
W(119)	2978		3074	2972	43	5	45	1	□ CH (50)
W(118)			3058	2957	6	1	149	3	υ CH (37)
W(117)		2920	3024	2924	62	8	106	2	υ CH(46)
W(116)	2904		3005	2906	42	5	119	3	υ CH (94)
W(115)	1634	1633	1693	1637	60	8	867	19	υ OC (67)
W(114)		1609	1677	1622	335	42	478	11	υ CC (54)
W(113)	1589		1643	1589	9	1	651	14	υ CC (45)
W(112)			1641	1587	93	12	551	12	υ CC (45)
W(111)			1626	1572	64	8	111	2	υ CC (36)
W(110)			1619	1566	29	4	36	1	υ CC (28)
W(109)			1602	1549	245	31	4532	100	υ OC (67)
W(108)		1520	1586	1534	800	100	1406	31	υ OC (36)
W(107)	1504	1510	1565	1513	109	14	31	1	υ CC (35)
W(106)			1547	1496	184	23	17	0	β HCC (44)
W(105)			1544	1493	86	11	27	1	β HCH (71)
W(104)			1538	1487	53	7	10	0	β HCH (77)
W(103)			1527	1477	11	1	26	1	β HCH (85)
W(102)			1519	1469	22	3	22	0	β HCH (72)
W(102)			1519	1469	22	3	22	0	β HCOC (47)
W(101)			1503	1453	14	2	27	1	β HCH (91)
W(100)			1496	1446	11	1	5	0	β HCH (34)
W(99)	1432	1431	1493	1444	17	2	120	3	β HCH (72)
W(98)	1406		1458	1410	28	4	44	1	β HCC (37)
W(97)			1451	1403	112	14	19	0	β HCC (36)
W(96)			1395	1349	149	19	107	2	β HCC (32)
W(95)		1331	1386	1340	60	8	137	3	β HCC (40)
W(94)			1372	1326	41	5	62	1	β HCC (42)
W(93)			1371	1326	49	6	394	9	β HCC (22)
W(92)			1366	1321	56	7	269	6	β HCC (40)
W(91)			1356	1311	18	2	425	9	β HCC (22)
W(90)	1282		1343	1299	3	0	32	1	β HCC (14)
W(89)			1316	1272	100	13	121	3	β HCC (22)
W(88)			1308	1265	145	18	62	1	β HCC (18)
W(87)			1306	1263	40	5	9	0	HCCC(39)
W(86)		1242	1296	1253	164	21	73	2	β HCC (11)
W(85)			1276	1234	231	29	182	4	υ OC (11)
W(84)	1230		1272	1230	242	30	190	4	β HCC(37)
W(83)	1210		1268	1226	1	0	29	1	β HCC(44)
W(82)		1187	1220	1180	174	22	4	0	β HOC(22)
W(81)			1210	1170	54	7	37	1	τ HCOC (26)

(*continued on next page*)

Table 2 (*continued*)

Species	Observed Wavenumbers(cm-1)		Theoretical wave number (cm-1)		IR Intensity		Raman Intensity		
	FTIR	FT RAMAN	Unscaled Frequency	Scaled Frequency	Rel	Abs	Rel	Abs	Vibrational Assignments
W(80)			1210	1170	62	8	78	2	τ HCOC (30)
W(79)			1200	1160	32	4	5	0	β HOC (17)
W(78)			1196	1157	7	1	13	0	τ HCOC (29)
W(77)	1146		1190	1150	119	15	3	0	τ HCOH (11)
W(76)			1167	1128	474	59	75	2	υ CC (33)
W(75)			1160	1122	0	0	5	0	τ HCOC (37)
W(74)	1113		1157	1119	9	1	12	0	β HCH (15)
W(73)			1128	1090	150	19	27	1	B CCC (21)
W(72)			1124	1087	404	51	61	1	β HOC (13)
W(71)	1028		1098	1062	124	16	370	8	τ HCCC (74)
W(70)			1050	1015	52	7	18	0	τ HCCC (74)
W(69)			1049	1015	57	7	6	0	τ HCCC (39)
W(68)			1031	997	55	7	9	0	β CCC (21)
W(67)		976	1029	995	57	7	20	0	β CCC (22)
W(66)	949		971	939	124	16	43	1	υ CC (14)
W(65)			961	929	1	0	25	1	τ HCCC (22)
W(64)			957	925	2	0	13	0	τ HCCC (23)
W(63)			948	917	7	1	2	0	τ HCCC (14)
W(62)			946	915	9	1	10	0	τ HCCC (15)
W(61)			939	908	27	3	34	1	τ HCCC (13)
W(60)			930	899	52	7	6	0	τ HCCC (27)
W(59)			924	893	6	1	9	0	υ CC (33)
W(58)			914	884	20	2	2	0	τ HCCC (39)
W(57)			902	873	16	2	1	0	τ HCCC (16)
W(56)	854	843	884	855	19	2	1	0	τ HCCC (66)
W(55)	807		837	809	7	1	3	0	τ HCCC (22)
W(54)			826	799	31	4	1	0	τ HCCC (46)
W(53)			817	790	65	8	15	0	τ HCCC (45)
W(52)			808	781	25	3	13	0	υ OCC (16)
W(51)			788	762	0	0	36	1	υ CC (11)
W(50)	722		759	734	15	2	10	0	υ CC (39)
W(49)			742	717	5	1	18	0	υ CC (17)
W(48)			728	704	1	0	3	0	σ OCCC (16)
W(47)			725	701	3	0	1	0	τ CCCC (52)
W(46)	630	657	679	657	29	4	2	0	σ OCCC (15)
W(45)			647	626	2	0	3	0	σ OCCC (36)
W(44)			634	613	7	1	1	0	τ CCCC (15)
W(43)			609	589	21	3	6	0	σ OCCC (25)
W(42)	572		599	579	15	2	6	0	β CCC (45)
W(41)		568	589	570	3	0	2	0	τ CCCC(25)
W(40)	533		563	544	9	1	3	0	β OCC (21)
W(39)	513		541	523	45	6	14	0	β OCC (13)
W(38)			524	507	15	2	2	0	β OCC (17)
W(37)			506	489	43	5	9	0	β CCC (14)
W(36)		467	493	477	6	1	2	0	β CCC (22)
W(35)			478	462	8	1	1	0	σ OCCC (11)
W(34)			474	458	1	0	1	0	σ OCCC (47)
W(33)			455	440	14	2	6	0	β CCC (31)
W(32)			423	409	7	1	3	0	β OCC (18)
W(31)			404	391	2	0	2	0	σ CCCC (18)
W(30)			386	373	20	3	4	0	σ CCCC (12)
W(29)			374	362	128	16	3	0	τ CCCC (10)
W(28)			362	350	144	18	4	0	τ HOCC (90)
W(27)			346	334	3	0	2	0	τ HOCC (94)
W(26)			341	330	11	1	4	0	β COC (22)
W(25)			304	294	7	1	1	0	β COC (26)

(*continued on next page*)

Table 2 (*continued*)

Species	Observed Wavenumbers(cm-1)		Theoretical wave number (cm-1)		IR Intensity		Raman Intensity		
	FTIR	FT RAMAN	Unscaled Frequency	Scaled Frequency	Rel	Abs	Rel	Abs	Vibrational Assignments
W(24)			291	281	1	0	0	0	β CCC (13)
W(23)			288	278	9	1	4	0	β OCC (31)
W(22)			284	274	2	0	1	0	β OCC (31)
W(21)			235	228	2	0	8	0	τ CCCC (12)
W(20)			231	224	3	0	4	0	β CCC (11)
W(19)		220	230	222	1	0	1	0	β CCC (23)
W(18)			210	203	1	0	3	0	β CCC (25)
W(17)			206	199	0	0	11	0	β OCC (30)
W(16)			181	175	3	0	2	0	τ CCCC (21)
W(15)			169	164	1	0	6	0	τ CCCC (42)
W(14)			154	149	1	0	9	0	τ CCCC (42)
W(13)			143	139	4	0	3	0	τ CCCC (11)
W(12)			125	121	1	0	3	0	τ CCCC (18)
W(11)		91	94	91	2	0	1	0	τ COCC (45)
W(10)			92	89	11	1	3	0	β CCC (18)
W(9)			88	85	10	1	1	0	β CCC (16)
W(8)			77	75	2	0	1	0	σ CCCC (17)
W(7)			68	66	3	0	0	0	τ CCCC (37)
W(6)			54	52	2	0	1	0	σ CCCC (14)
W(5)			51	49	0	0	2	0	β CCC (16)
W(4)			28	27	3	0	1	0	τ CCCC (30)
W(3)			15	15	0	0	6	0	τ CCCC (15)
W(2)			12	11	1	0	12	0	τ CCCC (59)
W(1)			3	3	1	0	8	0	τ CCCC (64)

1. υ -Symmetric Stretching, γ -Asymmetric stretching, β-symmetric bending, τ-Torsion and σ - Out.
2. Scaling Factor 0.961 for B3LYP6-311++G (d,p), taken from [Ref.13].
3. Relative absorption intensity normalized with highest peak absorption equal to 100.
4. Relative Raman intensity normalized to 100.

$$\text{Chemical Hardness}(\eta) = \frac{1}{2}(E_{LUMO} - E_{HOMO}) \quad (2)$$

$$\text{Chemical softness}(S) = \frac{1}{2}\eta \quad (3)$$

$$\text{Electronegativity } (\chi) = -\frac{1}{2}(E_{LUMO} + E_{HOMO}) = -\mu \quad (4)$$

$$\text{Electrophilicity } (\omega) = \frac{\mu^2}{2\eta} \quad (5)$$

(Figure 3) shows the existence of intramolecular charge move inside the molecule. The band gap energy estimation of the 7B3M5D molecule was determined as 4.464 eV. The ionization potential (IP) value demonstrates that energy value of 6.601 eV which is needed to expel an electron from the HOMO. The lower value of electron affinity demonstrates the higher molecular reactivity with nucleophiles. The lower softness value 0.223 eV [30, 31, 32] and higher chemical harness value 2.234 eV affirm the higher molecular hardness correlated with the molecule. The electrophilicity index insists the bioactivity and this affirms the signaling pathway for molecular docking studies of the target protein.

3.4. Mulliken atomic charge

The Mulliken atomic charge distribution provides a simple qualitative picture of chemists and is effective for B3LYP functional which is calculated using 6–311++G (d,p) level of theory [33] and is presented in (Figure 4). In general, Charge distribution and different methods have been improved to calculate them by quantum chemical calculation of the molecular system. Mulliken atomic charge is an extensively used charge partitioning scheme. Mulliken Atomic charge affects molecular polarizability, dipole moment, molecular reactivity, electronic structure of a molecular system. (Table.4) and (Figure 4) are analyzed and it shows that carbon atom C4 and C17 have a maximum negative charge, while all the hydrogen atoms have positive charges. Figure 4 shows Mulliken Population Analysis (MAP) atomic charges in increasing order of nucleophilic case C3>C5>C22 > C13 > C12 and C21. The order of electrophilic cases found to be C4>O27 > O18 > O25 > O16 > O8>O9 atom. The nucleophilic attacks generally assume a significant role in the biochemistry field [34].

3.5. Fukui Function analysis

Local quantities like Fukui function, local softness and Electrophilicity indices are calculated to analyze the reactivity/selectivity of the particular site in a molecule [35]. The individual atomic charges determined by Mulliken atomic charge are utilized to compute the Fukui function. In the present work, local descriptors like, the Fukui function (f_r^+,f_r^-,f_r^0), local softness (sr^+, sr^- and sr^0) and electrophilicity indices (ωr^+, ωr^- and ωr^0) for preferred atomic sites in 7B3M5D have been presented in (Table 4) [36, 37]. It has been discovered that Mulliken atomic charge plan predicted that O27 has a higher value which illustrates the probable locales for the electrophilic attack. Table 4 represents f_r^+ possess nucleophilic attack have been found around C4, C6, C3, C5, C2, C17, O18, C19 and C21 atoms for 7B3M5D. The (f_k^-) electrophilic attacks have been found around O8 and O9 atoms.

Table 3. Calculated HOMO-LUMO energy values of the 7B3M5D.

Molecular descriptors	Energy value (eV)
HOMO energy(E_{HOMO})	-6.601
LUMO energy(E_{LUMO})	-2.132
Energy gap (E_g)	4.464
Ionization potential (I)	6.601
Electron affinity(A)	2.132
Electronegativity (χ)	4.366
Chemical potential (μ)	-4.366
Chemical Hardness (η)	2.234
Chemical softness (S)	0.223
Electrophilicity index (ω)	3.818

3.6. NBO analyses

Natural bond orbital (NBO) analysis helps in sensing the intermolecular and intramolecular bonding interaction within the molecule [38]. It is a good tool to interrogate charge transfer within molecular systems. This gives molecular stability. The electron donor (i)-electron acceptor (j) and their stabilization energy E(2) are defined by the second-order perturbation concept (Equation 6) [39].

$$E(2) = \Delta E_{ij} = q_i (F_{ij})^2 / (E_j - E_i) \quad (6)$$

Where, q_i is the donor orbital occupancy, E_i, E_j are diagonal elements and F (i, j) is the Fock matrix for i and j NBO orbitals. The corresponding results are given in (Table 5). The molecular interaction is established between (C–C) σ and (C–C) σ* bond orbital whose result gives intramolecular charge transfer leading to stabilization of the system. The π-π* interactions of (C10–C15) π → (C13– C14) π*, (C23–C24) π → (C21–C22) π* and (C13–C14) π to (C11–C12) π* give rise to high stabilization energy values (21.90, 21.47 and 21.40 kcal/mol). The charge transfer from (C1–C2)σ,(C2–C3)σ*,(C7–H33) σ* and (C6–H32) σ* have less stabilization energy and the values are (2.00,4.45, 5.32 and 5.77 Kcal/mol). The other interactions in the 7B3M5D molecule involve electron-donating from LP(2) of Oxygen atoms O8, O9, O16, O18, O25 and O27 to the σ* and π* orbitals. The occupancy of LP(O8) → (C2–C3) σ*, LP(O9) → (C4–C5) σ*, LP(O16) → (C11–C12)π*, LP(O18) → (C13–C14) π*, LP(2)O25 → (C26–H45) π* orbitals and LP(O27) to (C21–C22) π* with stabilization energy of (20.99, 23.18, 25.96, 8.91,6.89 and 8.59 kcal/mol) respectively.

3.7. Molecular electrostatic potential

The molecular electrostatic potential (MEP) diagram is a very useful descriptor in understanding sites for nucleophilic and electrophilic properties [40, 41]. The MEP expresses the shape, size, reactive site and charge density of the molecule. The Molecular Electrostatic Potential of the 7B3M5D molecule was determined in this work by using the B3LYP functional with employing 6–311++G (d,p) level of theory and has color grid range between -7.852 × 10^{-2} eV to 7.852 × 10^{-2} eV. MEP surface is drawn for the title molecule by using the software Gaussview 5.0 program as represented in (Figure 5). The maximum negative region, which is a preferred site for electrophilic reactivity is shown in red and yellow region. The maximal positive charge region is expressed in blue, the maximum negative charge region is expressed in red and the green region is

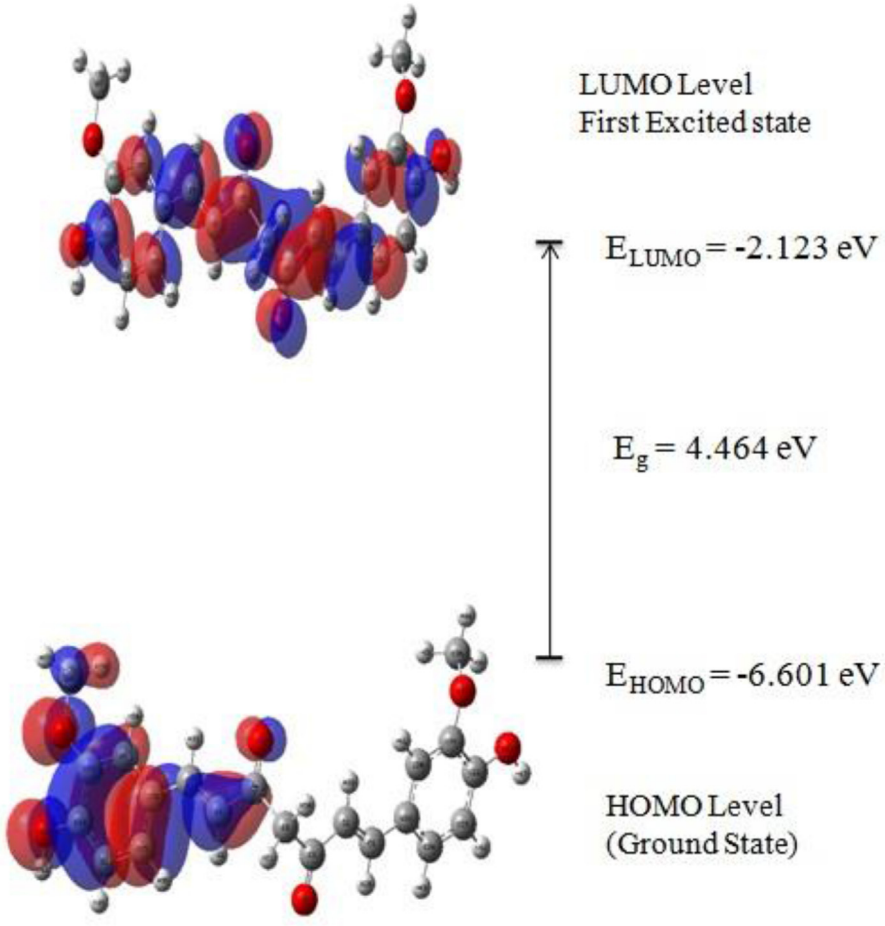

Figure 3. The atomic orbital composition of the frontier molecular orbital 7B3M5D.

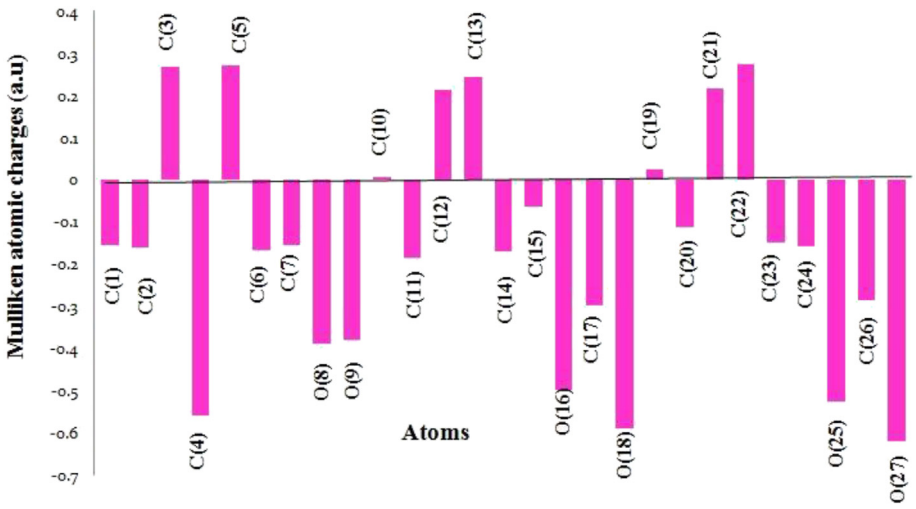

Figure 4. Mulliken atomic charge distribution of 7B3M5D molecule.

represented by neutral. In the MEP map, the negative district is more concentrated around the O(8),O(9), O(16), O(18), O(25) and O(27) atoms. Similarly oxygen atoms present in Mulliken outline additionally have negative electrostatic district. These results show that the nucleophilic and electrophilic sites are destinations for the binding site of the title compound.

3.8. ADMET prediction

Drug candidates should possess favorable ADMET prediction. The ADMET for 7B3M5D molecule is determined utilizing the pkCSM-ADME program which is an accessible web interface (http://structure.bioc.cam.ac.uk/pkcsm) an important tool to enable medicinal scientists to discover the balance between pharmacokinetic, potency, and toxicity evaluation. The title compound was evaluated by their Absorption, Distribution, Metabolism, Excretion and Toxicity (ADMET) profile were analyzed and tabulated in (Table 6). Different ADMET properties are distinguished for 7B3M5D molecule like the different parameters represent as CaCo2 permeability, Human Intestinal Absorption (HIA), Skin permeability, P-gp substrate and Inhibitor I &II, Blood-Brain Barrier (BBB) permeability, VDss, Fraction unbounded and CNS permeability,

Table 4. Mulliken Atomic Charges, Condensed Fukui table f_r, descriptors (sf_r) and (ωf_r) for 7B3M5D.

Atoms	Mulliken Atomic Charges			Fukui Function			Local Softness			Electrophilicity Indices		
	N	N+1	N-1	f_r^+	f_r^-	f_r^0	$(sf)_r^+$	$(sf)_r^-$	$(sf)_r^0$	$(\omega f)_r^+$	$(\omega f)_r^-$	$(\omega f)_r^0$
C1	-0.154	-0.081	-0.148	0.073	-0.006	0.033	0.021	-0.002	0.010	0.094	-0.008	0.043
C2	-0.161	-0.134	-0.138	0.027	-0.022	0.002	0.008	-0.006	0.001	0.035	-0.029	0.003
C3	0.268	0.411	0.356	0.143	-0.088	0.027	0.041	-0.025	0.008	0.185	-0.115	0.035
C4	-0.558	-0.340	-0.278	0.218	-0.280	-0.031	0.063	-0.081	-0.009	0.283	-0.362	-0.040
C5	0.269	0.412	0.357	0.143	-0.089	0.027	0.041	-0.026	0.008	0.186	-0.115	0.035
C6	-0.166	-0.122	-0.140	0.044	-0.026	0.009	0.013	-0.008	0.003	0.057	-0.034	0.011
C7	-0.155	-0.088	-0.142	0.066	-0.013	0.027	0.019	-0.004	0.008	0.086	-0.017	0.035
O8	-0.388	-0.475	-0.572	-0.087	0.184	0.048	-0.025	0.053	0.014	-0.113	0.238	0.062
O9	-0.379	-0.431	-0.564	-0.052	0.185	0.066	-0.015	0.053	0.019	-0.067	0.240	0.086
C10	0.007	0.130	0.139	0.123	-0.132	-0.004	0.036	-0.038	-0.001	0.160	-0.171	-0.006
C11	-0.184	-0.170	-0.205	0.014	0.021	0.018	0.004	0.006	0.005	0.018	0.028	0.023
C12	0.213	0.367	0.329	0.153	-0.116	0.019	0.044	-0.033	0.005	0.199	-0.150	0.024
C13	0.243	0.330	0.269	0.087	-0.026	0.031	0.025	-0.007	0.009	0.113	-0.034	0.040
C14	-0.168	-0.118	-0.135	0.050	-0.033	0.008	0.014	-0.010	0.002	0.065	-0.043	0.011
C15	-0.064	-0.095	-0.142	-0.031	0.078	0.023	-0.009	0.022	0.007	-0.040	0.101	0.030
O16	-0.498	-0.478	-0.526	0.020	0.028	0.024	0.006	0.008	0.007	0.025	0.037	0.031
C17	-0.296	-0.107	-0.065	0.189	-0.230	-0.021	0.054	-0.066	-0.006	0.245	-0.299	-0.027
O18	-0.586	-0.481	-0.571	0.105	-0.015	0.045	0.030	-0.004	0.013	0.137	-0.020	0.058
C19	0.025	0.134	0.141	0.109	-0.116	-0.004	0.031	-0.034	-0.001	0.141	-0.151	-0.005
C20	-0.112	-0.153	-0.166	-0.042	0.054	0.006	-0.012	0.016	0.002	-0.054	0.070	0.008
C21	0.215	0.358	0.298	0.143	-0.083	0.030	0.041	-0.024	0.009	0.186	-0.107	0.039
C22	0.274	0.326	0.275	0.052	-0.001	0.026	0.015	0.000	0.007	0.067	-0.001	0.033
C23	-0.150	-0.129	-0.138	0.020	-0.012	0.004	0.006	-0.003	0.001	0.026	-0.015	0.006
C24	-0.157	-0.117	-0.147	0.040	-0.010	0.015	0.011	-0.003	0.004	0.051	-0.012	0.020
O25	-0.524	-0.506	-0.535	0.019	0.011	0.015	0.005	0.003	0.004	0.024	0.014	0.019
C26	-0.285	-0.084	-0.066	0.202	-0.220	-0.009	0.058	-0.063	-0.003	0.261	-0.285	-0.012
O27	-0.617	-0.523	-0.576	0.094	-0.041	0.027	0.027	-0.012	0.008	0.122	-0.054	0.034

Table 5. Second order perturbation theory analysis of Fock matrix in NBO for 7B3M5D.

Donor(i)	Type	ED/e	Acceptor(j)	Type	ED/e	E(2)[a] (kj mol^{-1})	E(j)[b]-E(i) (a.u)	F(i,j)[c] (a.u)
C1–C2	σ	1.981	C1–C19	σ*	0.028	2.00	1.16	0.043
C1–C2	π	1.889	C3–O8	π*	0.124	16.79	0.29	0.062
C1–C19	σ	1.966	C2–C3	σ*	0.070	4.45	0.98	0.060
C1–H28	σ	1.973	C2–H29	σ*	0.020	5.83	0.88	0.064
C2–H29	σ	1.979	C1–H28	σ*	0.021	5.33	0.9	0.062
C3–O8	π	1.975	C1–C2	π*	0.056	3.92	0.41	0.036
C5–C6	σ	1.979	C7–C10	σ*	0.029	4.42	1.03	0.060
C5–O9	π	1.994	C6–C7	π*	0.073	3.88	0.41	0.036
C6–C7	σ	1.981	C5–O9	π*	0.130	17.21	0.29	0.063
C6–C7	π	1.876	C10–C15	π*	0.384	7.99	0.31	0.048
C6–H32	σ	1.977	C7–H33	σ*	0.019	5.32	0.90	0.062
C7–H33	σ	1.976	C6–H32	σ*	0.022	5.77	0.89	0.064
C10–C11	σ	1.968	C12–O16	σ*	0.033	4.14	0.99	0.057
C10–C15	π	1.647	C6–C7	π*	0.073	8.69	0.30	0.049
C10–C15	π	1.971	C13–C14	π*	0.377	21.9	0.27	0.070
C11–C12	σ	1.974	C13–O18	σ*	0.024	3.62	1.00	0.054
C11–C12	π	1.673	C10–C15	π*	0.384	21.2	0.30	0.073
C12–C13	σ	1.973	C13–C14	σ*	0.377	4.27	1.28	0.066
C13–C14	σ	1.976	C10–C15	π*	0.384	19.1	0.30	0.069
C13–C14	π	1.668	C11–C12	π*	0.394	21.4	0.29	0.071
C14–H35	σ	1.975	C10–C15	σ*	0.025	4.25	1.08	0.061
C19–C20	π	1.654	C23–C24	π*	0.337	21.07	0.28	0.069
C21–C22	σ	1.971	C19–C20	π*	0.368	19.39	0.31	0.069
C23–C24	σ	1.972	C19–C20	π*	0.368	21.31	0.29	0.071
C23–C24	π	1.682	C21–C22	π*	0.409	21.47	0.27	0.070
O8	LP(2)	1.977	C2–C3	σ*	0.070	20.99	0.62	0.103
O8	LP(2)	1.876	C3–C4	σ*	0.064	23.07	0.60	0.107
O9	LP(2)	1.967	C4–C5	σ*	0.065	23.18	0.60	0.107
O9	LP(2)	1.876	C5–C6	σ*	0.070	20.96	0.62	0.104
O16	LP(2)	1.848	C11–C12	π*	0.394	25.59	0.32	0.086
O18	LP(2)	1.931	C13–C14	π*	0.377	8.91	0.40	0.058
O25	LP(2)	1.905	C26–H45	σ*	0.022	6.86	0.68	0.062
O27	LP(2)	1.932	C21–C22	π*	0.409	8.59	0.39	0.056

ED(e) is the electron density of donor and acceptor in the NBO analysis.
[a] *E*(2) means the energy of hyperconjugative interactions (stabilization energy).
[b] Energy difference between donor and acceptor *i* and *j* NBOs.
[c] *F*(*i*,*j*) is the Fock matrix element between *i* and *j* NBOs.

CYP models for substrate (CYP2D6, CYP3A4) or inhibitor (CYP1A2, CYP2C19, CYP2C9, CYP2D6 and CYP3A4), Total clearance, Renal OCT2 substrate, Max. tolerated dose. Toxicity of drugs based on nine predictors, AMES toxicity, hERG I inhibitor & II, Oral rat toxicity, Oral rat chronic toxicity, Hepatotoxicity, Skin sensitization, *T. Pyriformis* toxicity and Minnow toxicity [42]. The CaCo2 permeability and low permeability for skin is determined to evaluate the absorption of title molecule were found to be (-0.093 ns m^{-1}and -2.76 log kp), Hence Human Intestinal Absorption is the most significant factors in the ADMET properties for a drug molecule. The HIA between 70 to 100% determines good intestinal absorption for drug molecules are observed from the intestine into the blood-stream in the event of 7B3M5D molecule the obtain value was found to be 82.19 %, which is well absorbed for the human body [43, 44]. Distribution is one of the most significant parameters; some fundamental parameters for distribution enclose BBB permeability. The capacity of a drug to enter the brain is a significant boundary that should be considered to decrease side effects and toxicity and the calculated value for the 7B3M5D molecule is -0.562 [45]. Generally by Cytochrome P450 (CYP) enzyme plays a significant part in drug metabolism which is indicated as an inhibitor of (3A4, 1A2, 2C19, 2C9 and 3A4), therefore non-inhibitor (CYP2D6), and P-gp which are the most significant structures in human [46, 47]. Excretion also predicts to be non-substrate of organic cation transporter 2 (OCT2) of the title molecule. The toxicity of the AEMS test demonstrating negative shows that its non-carcinogenic and non-mutagenic molecule. it does not inhibit hERG-I and hERG-II, Acute oral rat toxicity (LD50) was seen as 1.833 mol/kg, Chronic oral rat toxicity (LOAEL) was seen as 2.228 log mg/kg_bw/day, does not produce hepatotoxicity, it does not cause skin sensitivity, 0.494 log ug/L causes *T. pyriformis* Toxicity and minnow toxicity of the title molecule was found to be -0.081 log mM [48, 49, 50]. All the parameters result indicates that the title compound has been the biological activity of the drug in future.

3.9. Drug-likeness properties

The important rule/filter of drug-likeness is “Rule of Five” suggested by Lipinski, which characterizes the five rules of orally active compounds for physicochemical properties [51]. As per Lipinski's rule of five, that the molecule is found to be orally bioactive with the following factors, MW (Molecular Weight) $\leq$ 500, octanol-water partition coefficient (Mi logp) is less than or equal to 5, HBD (Hydrogen Bond Donor) is less than or equal to 5 and HBA (Hydrogen Bond Donor) is less than or equal to 10 and PSA (Polar Surface Area) $\leq$ 120Å [52]. These molecular properties for the title compound were

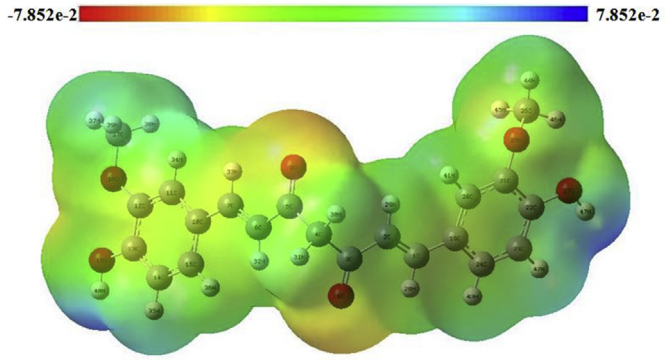

Figure 5. Molecular electrostatic potential (MEP) for the 7B3M5D molecule.

calculated using Molinspiration software which is freely accessible in web server tool (https://www.molinspiration.com). The estimated drug-likeness properties of the 7B3M5D molecule are listed in Table 7. Since the hydrogen bond donor is found to be ($2 \leq 5$), hydrogen bond acceptor is found to be ($6 \leq 10$), Molecular Weight $368.38 \leq 500$ g/mol, number of rotatable bonds (n_{rot}) $8 \leq 10$, and partition coefficient of title compound obtained the value of $2.3 \leq 5$. Finally molar refractivity and bioavailability score is 102.08, which is in the expected range between 40 to 130, while all the compounds obtained the bioavailability score of 0.55 [53]. The title compound is a better candidate for biological properties and hence applied for docking studies.

Table 6. Pharmacokinetic descriptors of pkCSM-ADMET properties for 7B3M5D.

Properties	Model Name	Predicted value
Absorption	Water solubility (log mol/L)	-4.01
	CaCo2 permeability (log Papp in 10^{-6} nm/s)	-0.093
	Human Intestinal Absorption (HIA) (% absorbed)	82.19
	Skin permeability (log kp)	-2.76
	P-glycoprotein substrate	Yes
	P-glycoprotein inhibitor I	Yes
	P-glycoprotein inhibitor II	Yes
Distribution	BBB permeability (log BB)	-0.562
	VDss (Human, log L/kg)	0.215
	Fraction unbounded (Fu)	0.16
	CNS permeability (log PS)	-2.99
Metabolism	CYP2D6 substrate	No
	CYP3A4 substrate	Yes
	CYP1A2 inhibitor	Yes
	CYP2C19 inhibitor	Yes
	CYP2C9 inhibitor	Yes
	CYP2D6 inhibitor	No
	CYP3A4 inhibitor	Yes
Excretion	Total clearance (log ml/min/kg)	-0.002
	Renal OCT2 substrate	No
	Max. tolerated dose (human)	0.081
Toxicity	AMES toxicity	No
	hERG I inhibitor	No
	hERG II inhibitor	No
	Oral rat toxicity (LD50) (mol/kg)	1.833
	Oral rat chronic toxicity (log mg/kg_bw/day)	2.228
	Hepatotoxicity	No
	Skin sensitization	No
	T.Pyriformis toxicity (log ug/L)	0.494
	Minnow toxicity (log mM)	-0.081

Table 7. Drug likeness parameters calculated for 7B3M5D molecule.

Descriptors	Values
Hydrogen bond donor (HBD)	2
Hydrogen bond acceptor (HBA)	6
Partition coefficient (Mi logP)	2.30
Molecular weight (MW) g/mol	368.38
Topological polar surface area (TPSA) ($Å^2$)	93.07
Number of atoms	47
Number of rotatable bonds	8
Molar refractivity	102.80
Bioavailability score	0.55

3.10. Molecular docking analyses

Molecular docking is a crucial tool for the computational simulation of a candidate ligand binding to a target receptor. The selected active site of the PI3K inhibitor of PDB ID (4FA6) was downloaded from RCSB [54] was to be docked with the 7B3M5D molecule. The resolution of protein with 2.70Å was selected for accurate data from the protein structure. The water molecules and ions are removed from the protein structure. Hydrogen atoms are added to the polar charges of the protein before docking studies. The grid box was centered on the binding site of the ligand and its size was set to coordinates are x, y and z (60 Å x 60 Å x 60Å) points with 0.375Å spacing respectively. Based on the 3D molecular structure of the title compound drawn using the Chemcraft tool and 7B3M5D optimized structure by using Gaussian 09 software with B3LYP method, after it is converted to PDB format was taken as a ligand for docking analysis. The prepared ligand-protein was docked by utilizing the Autodock program. From molecular docking studies generate ten conformers are used to obtain the best-fit conformer and its lowest binding energy. Docked conformation which had the lowest binding energy was selected to investigate the mode of binding. Among them, 4FA6 displays the lowest binding energy at -8.07 Kcal/mol with an inhibition constant of 277.94 μM with RMSD value 19.74 (Å) were listed in (Table 8). The active site residues are Tyr 867, Lys 890 and Val 882 at a distance 2.0, 1.9 and 2.5 (Å). (Figure 6) shows Cartoon representations of the ligand-protein complex and binding mode of interacting amino acid residues of 7B3M5D-PI3K/AKT inhibitor complex. The ligplot view shows hydrophobic and hydrogen bonding interaction in the active site of PI3K/AKT inhibitor as indicated in (Figure 7). The surface view of 7B3M5D encapsulated in the binding cavity of PI3K/AKT inhibitor is shown in (Figure 8). This result shows that the title compound has good agreement with the anti Non- Small Cell Lung Cancer agent for treating the PI3K/AKT inhibitor.

4. Molecular dynamics studies

Molecular dynamics studies are generated using the software GROMAS version 4.5.5 [55], Molecular dynamics (MD) simulation has been a significant part used to assess the structural dynamics of protein-ligand complex and their structural stability under solvent system [56, 57]. In this study, MD simulations were carried out for a timescale of 50 ns using the interaction of the protein-ligand complex. Topology parameter files for the Ligand 7B3M5D were prepared and executed using amber force field. Furthermore, analyses of root mean square deviation (RMSD), root mean square fluctuation (RMSF), Hydrogen bond, and interaction energy i.e. the sum of electrostatic and van der Waals interaction energies, are calculated with the aid of MD simulation.

4.1. Root mean square deviation (RMSD) analysis

To find the structural and conformational changes in the PI3K/AKT-ligand complex, molecular dynamics (MD) were carried out for 50 ns

Table 8. Hydrogen bonding and molecular docking with PI3K/AKT protein target-4FA6.

Protein (PDB ID)	Bonded residues	Bond distance (Å)	Estimated inhibition constant (μm)	Intermolecular energy (kcal/mol)	Binding energy (kcal/mol)	Reference RMSD (Å)
	Tyr867	2.0				
4FA6	Lys890	1.9	277.94	-11.31	-8.07	19.74
	Val882	2.5				

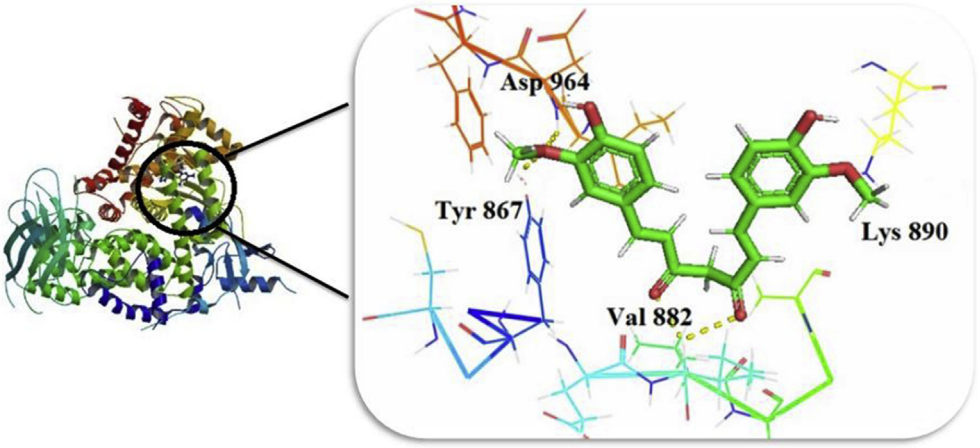

Figure 6. Cartoon representations of the ligand-protein complex and binding mode of interacting amino acid residues of 7B3M5D-PI3K/AKT inhibitor complex.

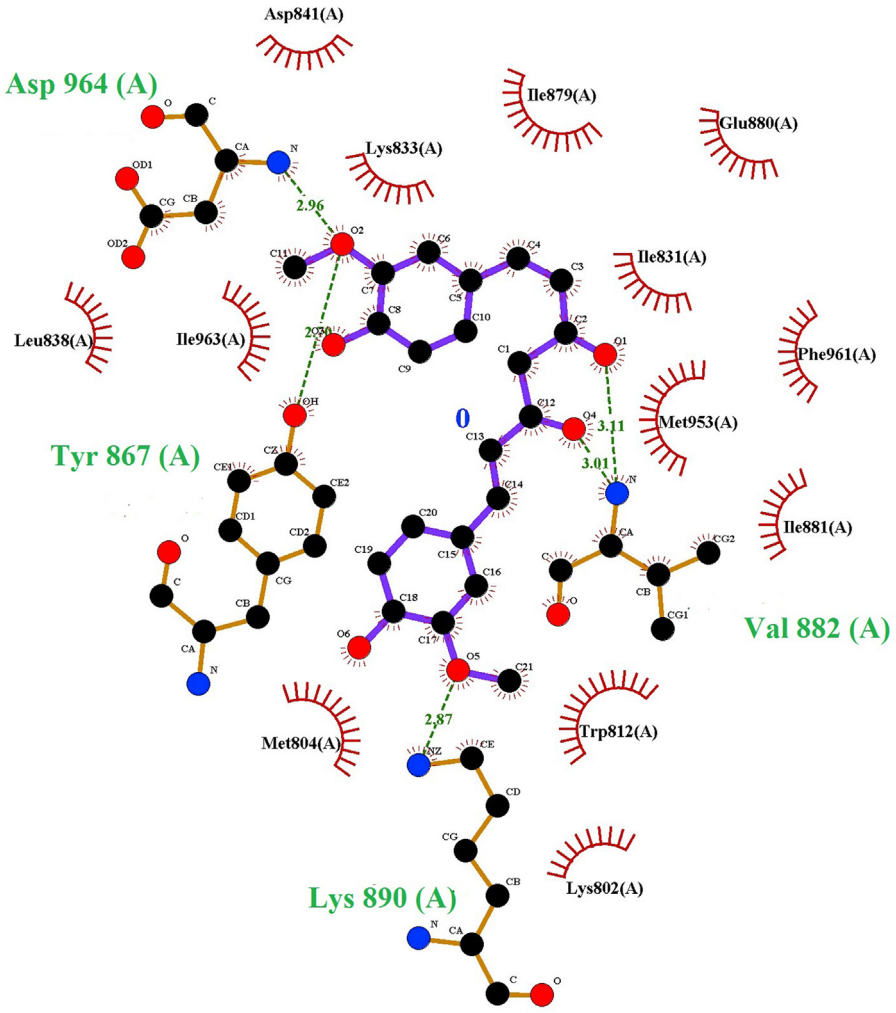

Figure 7. Ligplot view of hydrophobic and hydrogen bonding interaction in the active site of PI3K/AKT inhibitor.

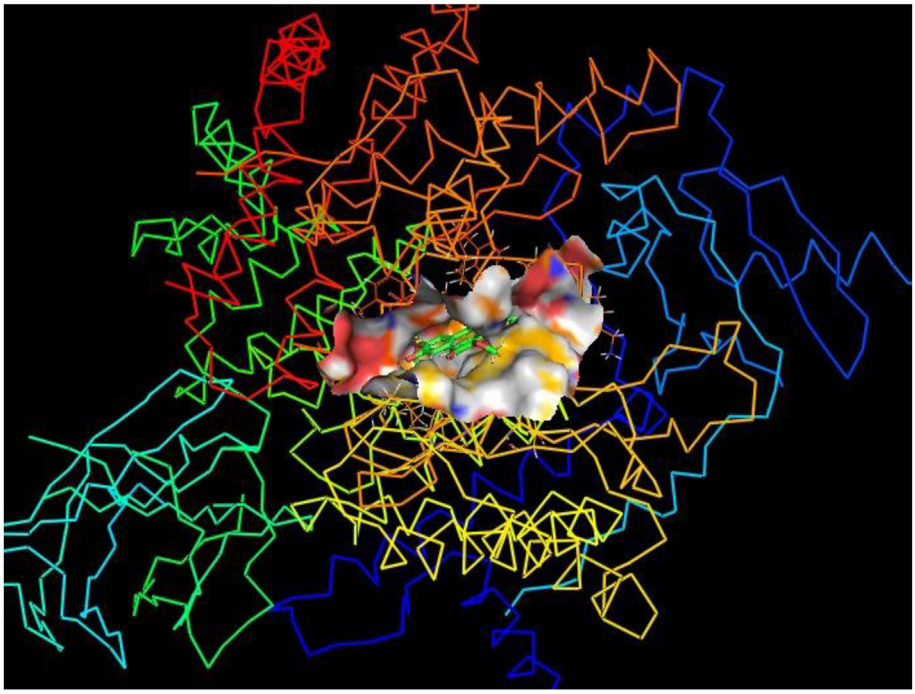

Figure 8. Surface view of encapsulated in the binding cavity of the 7B3M5D in the PI3/AKT inhibitor.

concerning time. (Figure 9) (a) shows the backbone atom RMSD of target and 7B3M5D bound PI3/AKT inhibitor complex. The protein-ligand complex (PI3K/AKT inhibitor-7B3M5D) maintains stability from 30 to 50 ns around 0.39 nm of RMSD backbone protein. From the plot, we can see that ligand 7B3M5D has higher stability with the protein binding cavity. The RMSD plot (Figure 9) (a) clearly shows that the ligand highly binds with the protein and maintains stability.

4.2. Root mean square fluctuation

The fluctuations of amino acid residues of target protein bound with the ligand 7B3M5D during the 50 ns simulation are shown in (Figure 9) (b). All residues have minimized Fluctuation and other of five residues with positions (200, 401, 580, 800, and 960). The five residues have high fluctuation and other residues have much-minimized fluctuation so the residues of ligand bounded protein fluctuation is very low and stable. Particularly, the interaction of amino acid residues in area 401–405 and 900–960 were profoundly fluctuated up to the most extreme of 0.1–0.55 Å and 0.1 to 0.5 in the target PI3K/AKT inhibitor-7B3M5D complex respectively.

4.3. Hydrogen bond and interaction energy analysis

The hydrogen bond formed between the interaction of protein-ligand complex, molecular stability, directionality and specificity are calculated based on the Molecular dynamics (MD) simulation [58]. The H-bond interaction between protein and ligand increases at the 50ns of MD simulation comparing to the initial structure (0 ns) [59, 60]. The inhibitor (protein)-7B3M5D (ligand) interaction was determined during the 50 ns in MD simulation. The ligand is stable with the protein and two H-bond from 50 to 20 ns of MD simulation. The corresponding hydrogen bonding (due to green color) of y-Axis increases from 2-3 number of hydrogen bond pair (due to magenta color) as shown in Figure 10 (a) in the MD simulation.

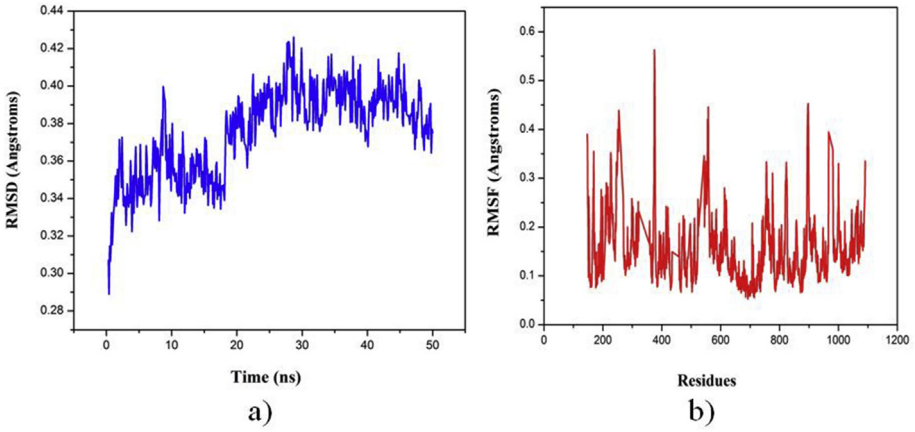

Figure 9. a) Root Mean Square Deviation (RMSD) plot of the backbone atom for PI3K/AKT inhibitor- 7B3M5D complex (b) the RMSF of the amino acid residues of target PI3K/AKT-7B3M5D complex during MD simulation.

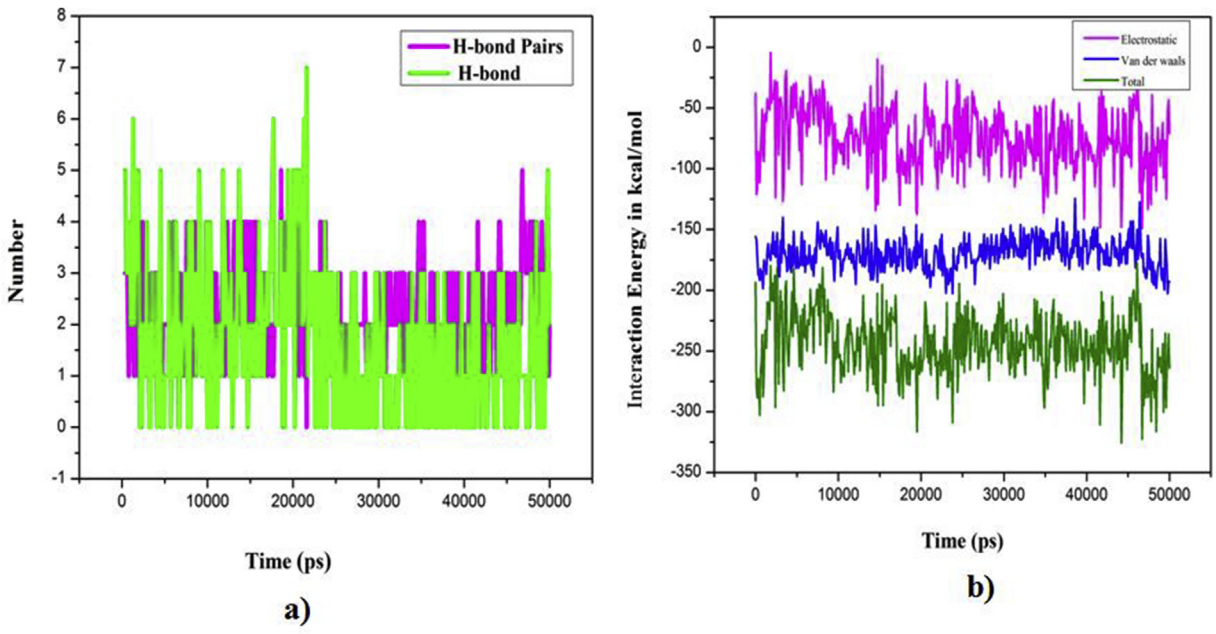

Figure 10. a) Hydrogen bonding interaction of complex b) The Interaction Energy of PI3K/AKT inhibitor- 7B3M5D complex. The total (green), Van der Waals (blue) and Electrostatic (pink) interaction energy between PI3K/AKT in MD simulation.

(Figure 10) (b) represents the interaction energy which is the conventional van der Waals interaction energy (blue color) is very much higher than electrostatic energy. Van der Waals interaction energy plays a vital role for the protein to ligand complex to bind with the electrostatic interaction energy. Initially, the corresponding interaction energy is -250 kcal/mol and finally, it keeps up to 270 kcal/mol at the end of 50 ns of the MD simulation. The van der Waals interaction energy is 175 kcal/mol from 0 to 50 ns of MD simulation electrostatic interaction energy, initially have -60 kcal/mol and hence with -80 kcal/mol at the end of 50 ns of MD simulation. The interaction energy from initial to final increases negatively and this indicates that ligand possesses higher binding affinity.

5. Conclusion

In the present work, the vibrational assignments (FT-IR, FT-Raman) of 7B3M5D was obtained by using DFT functional with B3LYP/6–311++G (d,p) level of theory. The optimized geometrical parameters (bond length, bond angle) were determined using DFT functional and examination was made by comparing with experimental results. Vibrational assignments were supported by Potential Energy Distribution (%PED). The HOMO-LUMO energy difference was determined and found to be 4.464 eV for 7B3M5D. The title compound was recognized from Molecular Electrostatic Potential and Fukui function analysis, the C=O group is in a more electrophilic reactive region. The intermolecular hyper conjugative interactions are LP (O16) to π*(C11–C12) and (C2–C3) π to (C15–O22) π* shows the highest stabilization energy of 25.59 kJ/mol by using NBO analysis. Drug likeness properties like ADMET and Lipinski's rule of five recommend the biological activity of title compound. Molecular docking studies were done to predict the possibilities of protein (PI3K/AKT)-ligand (7B3M5D) binding site. Analysis of 7B3M5D of PI3K/AKT inhibitor revealed strong stability of the binding affinity which is analyzed by Molecular Dynamics (MD) simulation. The results show that the title compound can be utilized for treating Non-Small Cell Lung Cancer agents and showed the lowest binding energy is -8.07kcal/mol.

Declarations

Author contribution statement

M. Govindammal, M. Prasath: Conceived and designed the experiments; Performed the experiments; Analyzed and interpreted the data; Contributed reagents, materials, analysis tools or data; Wrote the paper.

S. Kamaraj, M. Selvapandiyan: Analyzed and interpreted the data; Contributed reagents, materials, analysis tools or data.

S. Muthu: Conceived and designed the experiments; Analyzed and interpreted the data; Contributed reagents, materials, analysis tools or data.

Funding statement

This research did not receive any specific grant from funding agencies in the public, commercial, or not-for-profit sectors.

Data availability statement

Data included in article/supp. material/referenced in article.

Declaration of interests statement

The authors declare no conflict of interest.

Additional information

No additional information is available for this paper.

References

[1] A. Jemal, F. Bray, M.M. Center, J. Ferlay, E. Ward, D. Forman, Global cancer statistics, Ca - Cancer J. Clin. 61 (2011) 69–90.
[2] B. Vanhaesebroeck, L. Stephens, P. Hawkins, PI3K signaling the path to discovery and understanding, Nat. Rev. Mol. Cell Biol. 13 (2012) 195–203.
[3] I.A. Mayer, C.L. Arteaga, The PI3K/AKT pathway as a target for cancer treatment, Annu. Rev. Med. 67 (2016) 11–28.

[4] C. Massacesi, E. Di Tomaso, P. Urban, C. Germa, C. Quadt, L. Trandafir, R. Tavorath, PI3K inhibitors as new cancer therapeutics: implications for clinical trial design, Onco. Ther. 9 (2016) 203–210.

[5] T. Simoncini, A. Hafezi-Moghadam, D.P. Brazil, K. Ley, W.W. Chin, J.K. Liao, Interaction of estrogen receptor with the regulatory subunit of phosphatidylinositol-3-OH kinase, Nature 407 (2000) 538–541.

[6] L.M. Neri, P. Borgatti, P.L. Tazzari, R. Bortu, A. Cappellini, G. Tabellini, A. Bellacosa, S. Capitani, A.M. Martelli, The phosphoinositide 3-kinase/AKT1 pathway involvement in drug and all-trans-retinoic acid resistance of leukemia cells, Mol. Canc. Res. 1 (2003) 234–246.

[7] Z. Guo, X. Yang, F. Sun, R. Jiang, D.E. Linn, H. Chen, C.G. Tepper, A novel androgen receptor splice variant is up-regulated during prostate cancer progression and promotes androgen depletion–resistant growth, Canc. Res. 69 (2009) 2305–2313.

[8] P.T. Le, H. Cheng, S. Ninkovic, M. Plewe, X. Huang, H. Wang, C.M.L. Rogers, Design and synthesis of a novel pyrrolidinyl pyridopyrimidinone derivative as apotent inhibitor of PI3Ka and mTOR, Bioorg. Med. Chem. Lett 22 (2012) 5098–5103.

[9] H.A. Vogel, J. Pelletier, Harmacol Curcumin biological and medicinal properties, J. Pharma (1815) 2–50.

[10] K.G. Caramori, I.M. Adcock, Therapeutic potential of phosphatidylinositol 3-kinase inhibitors in inflammatory respiratory disease, J. Pharmacol. Exp. Therapeut. 1 (2007) 1–8.

[11] M.J. Frisch, G.W. Trucks, H.B. Schlegel, G.E. Scuseria, J.V. Ortiz, J. Cioslowski, D.J. Fox, Gaussian 09, Revision E.01, Gaussian, Inc., Wallingford CT, 2009.

[12] M.H. Jamroz, Vibrational energy distribution analysis, VEDA 4, warsaw, Spectrochim. Acta. A 114 (2004) 220–230.

[13] Jacob George, Johanan Christian Prasana, S. Muthu, K. Tintu, S. Kuruvilla, Sevanthi, Rinnu Sara Saji, Spectroscopic (FT-IR, FT Raman) and quantum mechanical study on N-(2,6-dimethyl phenyl)-2-{4-[2-hydroxy-3-(2-methoxy phenoxy)propyl] piperazin-1- yl}acetamide, J. Mol. Struct. 1171 (2018) 268–278.

[14] A.E. Reed, L.A. Curtiss, F. Weinhold, Intermolecular interactions from a natural bond orbital, donor-acceptor viewpoint, Chem. Rev. 88 (1988) 899–926.

[15] M. Raja, R. Raj Muhamed, S. Muthu, M. Suresh, Synthesis, spectroscopy (FT- IR, FT-Raman, NMR, UV-Visible), first order hyperpolarizability, NBO and molecular docking study of (E)-1-(4-bromobenzylidene) semicarbazide, J. Mol. Struct. 1128 (2017) 481–492.

[16] O. Trott, A.J. Olson, Autodock vina, Improving the speed and accuracy of docking with a new scoring function, efficient optimization and multithreading, J. Comput. Chem. 31 (2010) 455–461.

[17] W.L. Delano, PyMol Molecular Graphics System, Delano Scientific, San Carlos, CA,USA, 2002.

[18] Joel T. Mague, William L. Alworth, Florastina L. Payton, Curcumin and derivatives, Acta Crystallogr. 60 (2004) 608–610.

[19] T. Sundius, Scaling of ab initio force fields by MOLVIB, Vib. Spectrosc. 29 (2002) 89–95.

[20] M. Govindammal, M. Prasath, S. Kamaraj, B. Sathya, Invivo, molecular docking, spectroscopy studiesof(S)-2,3-Dihydro-5,7-dihydroxy-2(3-hydroxy-4-methoxyphenyl)-4H-1-benzopyran-4-one: a potential uptake PI3/AKT inhibitor, Biocatal. Agri. Biotechnol. 18 (2019) 101086.

[21] M. Pagannone, B. Fornari, G. Mattei, Molecular structure and orientation of chemisorbed aromatic carboxylic acids: surface enhanced Raman spectrum of benzoic ac-id adsorbed onsilver sol, Spectrochim. Acta 43 (1987) 621–625.

[22] M. Prasath, M. Govindammal, B. Sathya, Spectroscopic investigations (FT-IR &FTRaman) and molecular docking analysis of 6-[1-methyl-4-nitro-1H-imidazole-5-yl) sulfonyl]-7H-purine, J. Mol. Struct. 1146 (2017) 292–300.

[23] K. Kesavan Muthu, A. Gunasekaranl, P. Kala, Govindasamy, P. Rajesh, P.P. Moorthi, Spectroscopic (FT-IR, FT-Raman & UV-vis) and density functional theory studies of cefadroxil, Int. J. Curr. Microbiol. App. Sci. 11 (2015) 211–225.

[24] P.S. Kalsi, Spectroscopy of Organic Compounds, Academic Press, New York, NY, 2002.

[25] Y. Erdogdu, O. Unsalan, M. Amalanathan, I. Hubert Joe, Infrared and Raman Spectra,Vibrational assignments ,NBO analysis and DFT calculations of 6-aminoflavone, J. Mol. Struct. 980 (2010) 24–30.

[26] S. Sakthivel, T. Alagesan, S. Muthu, C.S. Abraham, E. Geetha, Quantum mechanical ,spectroscopic study (FT-IR and FT-Raman), NBO analysis, HOMO-LUMO ,first order hyperpolarizability and docking studies of a non-steroidal anti-inflammatory compound, J. Mol. Struct. 1156 (2018) 645–666.

[27] D.F.V. Lewis, C. Ioannides, D.V. Parke, Interaction of a series of nitriles with the alcoholinducible isoform of P450: computer analysis of structure-activity relationships, Xenobiotica 24 (1994) 401–408.

[28] V. Karunakaran, V. Balachandran, FT-IR, FT-Raman spectra, NBO, HOMO–LUMO and thermodynamic functions of 4-chloro-3-nitrobenzaldehyde based on *ab initio* HF and DFT calculations, Spectrochim. Acta 98 (2012) 229–239.

[29] G.L. Eakins, J.S. Alford, B.J. Tiegs, B. Breyfogle, C.J. Stearman, Tuning HOMO –LUMO levels: trends leading to the design of 9-fluorenone scaffolds with predictable Electronic and optoelectronic properties, J. Phys. Org. Chem. 24 (2011) 1119–1128.

[30] B. Chandralekha, Rajagopal Hemamalini, S. Muthu, S. Sevvanthi, Spectroscopic (FT-IR, FT- Raman, NMR, UV-Vis) investigations, computational analysis and molecular docking study of 5-bromo-2-hydroxy pyrimidine, J. Mol. Struct. 1218 (2020) 128494.

[31] R. Mathammal, N. Jayamani, N. Geetha, Molecular structure, NMR, HOMO, LUMO, and vibrational analysis of O-anisic acid and anisic acid based on DFT calculations, J. Spectr. 18 (2013).

[32] Ralph G. Pearson, Absolute electronegativity and hardness correlated with molecular orbital theory, Proc. Natl. Acad. Sci. Unit. States Am. 83 (1986) 8440–8441.

[33] A. Bajpai, A.K. Pandey, K. Pandey, A. Dwivedi, Reactive nature, substitution reaction, structural and vibrational properties of 2, 3 dichloropridine by DFT study, J. Comput. Methods Mol. Des. 4 (2014) 64–69.

[34] S. Sevvanthi, S. Muthu, M. Raja, S. Aayisha, S. Janani, PES, molecular structure, spectroscopic (FT-IR, FT-Raman), electronic (UV-Vis, HOMO-LUMO), quantum chemical and biological (docking) studies on a potent membrane permeable inhibitor: dibenzoxepine derivative, Heliyon 6 (2020), e04724.

[35] P. Kolandaivel, G. Praveen, P. Selvarengan, Study of atomic and condensed atomic indices for reactive sites of molecules, J. Chem. Sci. 117 (2005) 591–598.

[36] S. Muthu, E. IsacPaulraj, Spcetroscopic and molecular structure (monomeric and dimeric structure) investigation of 2-[(2-hydroxyphenyl)crbonyloxy] benzoic acid by DFT method: a combined experimental, Structure 1038 (2013) 145–162.

[37] B. Sathya, M. Prasath, Spectroscopic (FT-IR, FT-Raman, UV-Vis), quantum chemical calculation and molecular docking evaluation of liquiritigenin: an influenza A (H1N1) neuraminidase inhibitor, Res. Chem. Intermed. 45 (2019) 2135–2166.

[38] P. Chattaraj, K. Maiti, B. Sarkar, A unified treatment of chemical reactivity and Selectivity, J. Phys. Chem. 107 (2003) 4973–4975.

[39] B. Sathya, S. Karthi, K. Ajaijawahar, et al., Probing the vibrational spectroscopic properties and binding mechanism of anti-influenza agent Liquiritin using experimental and computational studies, Res. Chem. Intermed. 46 (2020) 4475–4507.

[40] M. Prasath, S. Muthu, R. Arun Balaji, Vibrational spectroscopy investigation using ab initio and DFT vibrational analysis of 7-chloro-2-methylamino-5-phenyl-3H-1,4-benzodiazepine- 4-oxideSpectrochim Acta, A Mol. Biomol. Spectr. 113 (2013) 224–235.

[41] E. Scrocco, J. Tomasi, Electronic molecular structure, reactivity and intermolecular forces: an euristic interpretation by means of electrostatic molecular potentials, J. Adv. Quant. Chem 11 (1978) 115–193.

[42] E. Douglas, V. Pires, Tom L. Blundell, David B. Ascher, pkCSM: predicting Small-molecule pharmacokinetic properties using graph-based signatures, J. Med. Chem. 58 (2015) 4066–4072.

[43] S. Singh, J. Singh, Transdermal drug delivery by passive diffusion and iontophoresis: a review, Med. Res. Rev. 13 (1993) 569–621.

[44] Y.H. Zhao, J. Le, M.H. Abraham, A. Hersey, P.J. Eddershaw, C.N. Luscombe, et al., Evaluation of human intestinal absorption data and subsequent derivation of a quantitative structure-activity relationship (QSAR) with the Abraham descriptors, J. Pharm. Sci. 90 (2001) 749–784.

[45] M.S. Alavijeh, M. Christy, M.Z. Qaiser, A.M. Palmer, Drug metabolism and pharmacokinetics, the blood-brain barrier, and central nervous system drug discovery, NeuroRx 2 (2005) (2005) 554–571.

[46] A. Isvoran, Maxime Louet, Diana Larisa Vladoiu, Craciun Dana, Marie-Anne Loriot, Bruno O. Villoutreix, Maria A. Miteva, Pharmacogenomics of the cytochrome P450 2C family: impacts of amino acid variations on drug metabolism, Drug Discov. Today in press 22 (2017) 366–376.

[47] U.M. Zanger, M. Schwab, Cytochrome P450 enzymes in drug metabolism: regulation of gene expression, enzyme activities, and impact of genetic variation, Pharmacol. Ther. 138 (2013) 103–141.

[48] Ying Han, Jingpu Zhang, Chang Qin Hu, Xia Zhang, Bufang Ma, Peipei Zhang, In silico ADME and toxicity prediction of ceftazidime and its impurities, Front. Pharmacol. 10 (2019) 434.

[49] D.E. Pires, T.L. Blundell, D.B. Ascher, PkCSM: predicting small-molecule Pharmacokinetic and toxicity properties using graph-based signatures, J. Med. Chem. 58 (2005) 4066–4072.

[50] M. Tristani-Firouzi, J. Chen, J.S. Mitcheson, M.C. Sanguinetti, Molecular biology of K+ channels and their role in cardiac arrhythmias, Am. J. Med. 110 (2001) 50–59.

[51] C.A. Lipinski, F. Lombardo, B.W. Dominy, P.J. Feeney, Experimental and computational approaches to estimate solubility and permeability in drug discovery and development settings, Adv. Drug Deliv. Rev. 23 (1997) 3–25.

[52] M. Govindammal, M. Prasath, Vibrational spectra, Hirshfeld surface analysis, molecular docking studies of (RS)-N,N-bis(2-chloroethyl)-1,3,2-oxazaphosphinan-2-amine 2-oxide by DFT approach, Heliyon 6 (2020), e04641.

[53] A.K. Ghose, V.N. Viswanadhan, J.J. Wendoloski, A knowledge-based approach in designing combinatorial or medicinal chemistry libraries for drug discovery. 1. A qualitative and quantitative characterization of known drug databases, J. Combin. Chem. 1 (1991) 55–68.

[54] P. Furet, V. Guagnano, R.A. Fairhurst, P. Imbach-Weese, I. Bruce, M. Knapp, C. Fritsch, F. Blasco, J. Blanz, R. Aichholz, J. Hamon, D. Fabbro, G. Caravatti, Discovery of NVP-BYL719 a potent and selective phosphatidylinositol-3 kinase alpha inhibitor selected for clinical evaluation, Bioorg. Med. Chem. Lett 23 (2013) 3741–3748.

[55] B. Hess, C. Kutzner, D. Van der Spoel, E. Lindahl, GROMACS 4: algorithms for highly efficient, load balanced, and scalable molecular simulation, J. Chem. Theor. Comput. 4 (2008) 435–447.

[56] Saman Fatima, Taj Mohammad, Deeba Shamim Jairajpuri, Md. Tabish Rehman, Afzal Hussain, Mohammed Samim, Farhan Jalees Ahmad, Mohammed F. Alajmi, Md. Imtaiyaz Hassan, Identification and evaluation of glutathione conjugate gamma-L- glutamyl-L-cysteine for improved drug-delivery to the brain, J. Biomol. Struct. Dynam. 38 (2020) 3610–3620.

[57] S. Kannan, P. Kolandaivel, Computational studies of pandemic 1918 and 2009 H1N1 hemagglutinins bound to avian and human receptor analogs, J. Biomol. Struct. Dynam. 34 (2016) 272–289.
[58] R.E. Hubbard, M. Kamran Haider, Hydrogen bonds in proteins: role and strength, e *LS* (2001).
[59] Taj Mohammad, Kaynat Arif, Mohamed F. Alajmi, Afzal Hussain, Asimul Islam, Md. Tabish Rehman Md, Imtaiyaz Hassan, Identification of high-affinity inhibitors of pyruvate dehydrogenase kinase-3: towards therapeutic management of cancer, J. Biomole. Struct. Dynam. 14 (2020) 1–9.
[60] S. Kannan, P. Kolandaivel, The inhibitory performance of flavonoid cyanidin-3-sambubiocide against H274Y mutation in H1N1 influenza virus, J. Biomol. Struct. Dyn. 36 (2018) 4255–4269.